Top Catal (2012) 55:731–746
DOI 10.1007/s11244-012-9872-5

ORIGINAL PAPER

XPS–SIMS Surface Characterization of Aluminovanadate Oxide Catalyst Precursors Co-Precipitated at Different pH: Effect of Calcination

S. P. Chenakin · R. Prada Silvy · N. Kruse

Published online: 25 July 2012

Abstract X-ray photoelectron spectroscopy and time-of-flight secondary ion mass spectrometry were employed in a comparative study of the surface physical and chemical state of aluminovanadate oxide catalyst precursors (V–Al–O), which were precipitated in the range of pH from 5.5 to 10, after drying and calcination. Core-level photoelectron spectra, X-ray induced Auger and valence band spectra of the samples were measured so as to quantitatively evaluate the surface concentrations of the catalyst components. The binding energy shifts of the respective O 1s, V 2p and Al 2p lines were determined as a function of pH and analyzed in terms of the initial state effect related to the atomic charge and Madelung potential. The surface of the catalysts was composed of aluminum hydroxide/oxyhydroxide and of dispersed vanadium oxide species. Increasing pH was found to result in a monotonic variation of the elemental surface composition, modification of the valence band, progressive hydroxylation of the surface and increasing dispersion of vanadium oxide species. Increasing pH was also accompanied by an increase in the abundance of V^{4+} species, specific surface area and reducibility. Calcination in air at 500 °C gave rise to surface segregation of vanadium, changes in the valence band and partial dehydroxylation. The structural transformations in vanadium oxide species and aluminium hydroxide support and their interaction were accompanied by an increasing abundance of V–O–Al bonds. The net result of the restructuring was a decrease in the specific surface area and reducibility of the calcined catalysts. The enhancement of the catalytic activity in propane oxidative dehydrogenation demonstrated by V–Al–O samples with increasing precipitation pH and after calcination was in good correlation with a growing population of the V^{4+} states and increasing nucleophilicity of oxygen sites.

Keywords Aluminovanadate oxide catalyst (V–Al–O) · XPS · ToF-SIMS · Vanadium oxidation state · Propane ODH

S. P. Chenakin · N. Kruse (✉)
Chimie-Physique des Matériaux, Université Libre de Bruxelles (ULB), CP 243, 1050 Brussels, Belgium
e-mail: nkruse@ulb.ac.be

Present Address:
S. P. Chenakin
Institute of Metal Physics, Nat. Acad. Sci., Akad. Vernadsky Blvd. 36, Kiev-142 03680, Ukraine

R. P. Silvy
Unité de Catalyse et Chimie des Matériaux Divisés, Université Catholique de Louvain, Croix du Sud, 2/17, 1348 Louvain-La-Neuve, Belgium

1 Introduction

For decades, vanadium oxide based catalytic systems have been investigated extensively and have received great attention in the catalysis literature because of intense interest in their multiple industrial applications [1, 2]. In particular, among the various catalysts proposed for the reaction of oxidative dehydrogenation (ODH) of alkanes, which offers an energetically attractive route for the production of alkenes, vanadium oxide based catalysts are the most promising and frequently studied [3].

The catalytic properties of vanadium-containing oxide materials depend greatly on the preparation method and the support. Studies of the influence of various preparation methods on the performance of bulk V–Nb–O and niobia supported vanadium oxide catalysts [4, 5] have shown that the preparation method has a drastic effect on the surface

concentration of vanadia. Although the catalysts demonstrated widely different activities for ODH of propane per gram of catalyst, the activity per surface vanadium was more or less constant. This led to the suggestion that the activation of propane takes place on a vanadium site at the surface and all the vanadium oxide catalysts contain essentially the same vanadium oxide configurations. I. Wachs has recently generalized [6] that all V-containing supported and mixed oxide catalytic materials are characterized by the universal presence of surface VO_x sites, which are catalytic active.

Various pre-treatments of vanadium-based catalysts can be performed which are aimed at improving their catalytic properties, with calcination being a usual step in preparing a stable catalyst. A number of works have been devoted to studying the effect of the calcination temperature on the surface structure and catalytic performance of vanadium oxide materials. For V_2O_5/Nb_2O_5 catalysts, the specific activity in ODH of propane was observed to increase with increasing calcination temperature from 550 to 700 °C; however, at 750 °C a new phase, (VNb_9O_{25}), was formed which decreased the activity [4]. In VO_x/ZrO_2 catalysts, the calcination temperature (500 and 650 °C) was found to influence the nature of surface vanadium oxide species, the surface V/Zr atomic ratio and the catalytic performance in the propane ODH. After calcination at 650 °C a loss of activity due to formation of ZrV_2O_7 was reported [7]. In contrast to V_2O_5/TiO_2 catalysts, which demonstrated a decrease in propene yield with increasing calcination temperature in the range 450–800 °C, the V_2O_5 (2 wt %)/50 % TiO_2–SiO_2 catalyst was found to maintain the same propane ODH activity up to the highest calcination temperature [8].

X-ray photoelectron spectroscopy (XPS) analysis of supported catalysts, V_2O_5/TiO_2–ZrO_2 [9] and V_2O_5/Al_2O_3–TiO_2 [10], calcined in flowing O_2 at different temperatures in the range 500–800 °C revealed developing modification of the surface composition and the oxidation state of vanadium indicated by an increase in the surface V/Ti atomic ratio and V $2p_{3/2}$ binding energy with increasing calcination temperature and implied formation at high temperatures of the ZrV_2O_7 phase as a result of selective interaction of dispersed vanadium oxide with a particular component of the mixed oxide support in the V_2O_5/TiO_2–ZrO_2 system. On the contrary, in the V_2O_5/Ga_2O_3–TiO_2 catalyst [11], the surface V/Ti atomic ratio and V $2p_{3/2}$ binding energy were observed to decrease with increasing calcination temperature. In the V_2O_5/La_2O_3–TiO_2 catalytic system [12] calcined at 500 and 800 °C, predominance of the V^{4+} reduced species and formation of the $LaVO_4$ phase was observed. For all the above catalysts [4, 7–12] the increase in calcination temperature gave rise to a decrease in the specific surface area. While information on modification of the surface composition of the supported catalysts as a function of calcination temperature can be found in the literature [7, 9–12], no data is available on the surface composition of dried catalysts to see how it changes after calcination.

Quantitative XPS analysis of supported vanadyl phosphate catalysts $VOPO_4/Al_2O_3$, $VOPO_4/TiO_2$ [13] and $Fe_{0.2}(VO)_{0.8}PO_4/Al_2O_3$ [14] showed that a progressive reduction of vanadium species occurred in the samples with an increase in the temperature of calcination in the range 450–650 °C. Besides, an increase in the content of titanium and aluminium phosphates formed in the $VOPO_4/Al_2O_3$ and $VOPO_4/TiO_2$ systems was observed as the temperature of calcination increased. The catalytic activity of the $VOPO_4/Al_2O_3$ and $Fe_{0.23}(VO)_{0.77}PO_4/Al_2O_3$ catalysts in ODH of ethane at a given temperature was found to generally increase with an increase in the calcination temperature, whereas ethylene selectivity was not significantly affected by the calcination temperature [15].

The aluminovanadate oxide (V–Al–O) prepared by co-precipitation was reported [16] to be an active and relatively selective catalyst for the ODH of propane (propane conversion amounted to 44 %), with its activity being presumably controlled by the redox capacity of V ions [17]. The activity of vanadium–aluminium oxynitride catalysts (V–Al–O–N) prepared by nitridation of V–Al–O at 500 °C in the flow of NH_3 was much lower than that of the oxide precursor and was constant irrespective of the V/Al ratio and nitrogen content [18]. On the other hand, the V–Al–O–N catalyst was found to exhibit excellent properties in the propane ammoxidation process demonstrating a high acrylonitrile yield at a very short contact time [19]. The catalytic properties of the V–Al–O–N catalysts can be strongly influenced by the preparation conditions. In particular, the acrylonitrile yield was observed to depend on drying or calcination temperature of the V–Al–O precursor prior to the catalytic test performed under propane ammoxidation reaction conditions (reaction temperature 500 °C; NH_3:O_2:C_3H_8 = 1:3:1.25) [20]. In situ valence-to-core X-ray emission spectroscopy study [21] performed under propane ammoxidation conditions revealed a gradual decrease of the formal oxidation state of vanadium in the precursor V–Al–O catalyst during 9 h on-stream in the catalytic environment from +4.8 to +3.8.

Of the various parameters influencing the catalytic performance of aluminovanadate oxide precursors, the pH value of co-precipitation seems to play a crucial role. In previous works [16, 17] the effect of the co-precipitation pH on the physicochemical and catalytic properties of these materials was investigated. The aim of the present study is to carry out, using a combination of XPS and time-of-flight secondary ion mass spectrometry (ToF-SIMS), a comprehensive surface characterization of aluminovanadate oxide

catalysts synthesized at different precipitation pH in order to determine how the preparation conditions affect the physicochemical characteristics, surface composition and electronic structure of dried catalysts, to realize how they change after calcination and to relate the data obtained to the catalytic activity of the material.

2 Experimental

Aluminovanadate oxide catalyst precursors V–Al–O were prepared [16] by co-precipitation of aluminium nitrate $Al(NO_3)_3{\cdot}9H_2O$ (0.080 M) and ammonium metavanadate NH_4VO_3 (0.030 M) aqueous solutions at pH of 5.5, 7.5, 8.5 and 10.0 adjusted by addition of a NH_4OH solution. The V/Al atomic ratio in the catalysts was fixed at 0.25, which was shown [22] to furnish the best catalytic properties. The precipitate was filtered, washed several times with hot water and dried at 60 °C for 4 h and at 120 °C overnight, yielding finally a powder with an average size of the particles in the range 175–230 μm depending on pH [16]. The samples prepared in this way and denoted hereafter as 'dried' were then subjected to heat treatment in air at 500 °C for about 2 h to produce 'calcined' precursors.

The specific surface area of the catalysts was measured from the N_2 adsorption isotherm at 77 K in a Micromeritics Flow-Sorb II 2300 apparatus. The reducibility of the V–Al–O catalysts was studied by temperature-programmed reduction using ChemBET 3000 equipment with a tubular reactor. Samples of about 50 mg were first pretreated in flowing He (30 ml/min) at 200 °C for 1 h to eliminate residual moisture and then heated at a rate of 10 °C/min up to 900 °C in a flow of 5 % H_2 + Ar mixture (20 ml/min). Hydrogen consumption was determined on the basis of a calibration performed with CuO and was expressed in terms of a milli-mole of consumed H_2 per gram of catalyst.

Activity tests for the propane oxidative dehydrogenation reaction were conducted in a fixed bed micro-reactor coupled on-line to a gas chromatograph under the following experimental conditions: amount of catalyst 100 mg, reaction temperature 460 °C, total pressure 10^5 Pa, and a feed composition C_3:O_2:He = 10.0:7.5:82.5 ml/min.

For XPS and SIMS analyses, the powder of dried and calcined V–Al–O samples was pressed uniformly over an indium film on a flat sample holder to form a layer typically about 0.1 mm thick. Experiments were performed in a combined XPS-ToF-SIMS instrument at a base pressure of 8.1×10^{-10} mbar. For XPS, a non-monochromatic Mg K_α radiation of a source operating at a power of 150 W was employed. Prior to analysis, the samples were kept for degassing in a preparation chamber at a base pressure of 5×10^{-10} mbar for 48–96 h. Photoelectron core-level spectra were acquired using a hemispherical analyzer at a pass-energy of 50 eV with a 0.05 eV energy step. The overall resolution of the spectrometer in this operating mode was 0.96 eV measured as a full width at half maximum (FWHM) of the Ag $3d_{5/2}$ line. The spectrometer was calibrated against E_b(Au $4f_{7/2}$) = 84.0 eV. The Al KLL Auger spectra were excited by the Bremsstrahlung radiation. Previous experiments have shown [23] that the surface of the V–Al–O catalysts happened to be rather sensitive to X-ray irradiation and suffered structural and chemical damage under extended X-ray exposure. To minimize X-ray damage of V–Al–O, acquisition of core level spectra was started immediately after exposing the sample to the operating X-ray source and the exposure was kept as low as possible.

After subtracting the Shirley-type background, the Al 2p, V 2p and O 1s core-level spectra were curve-fitted with mixed symmetrical Gaussian–Lorentzian (G–L) lines by a least-squares fit procedure, using the public software package XPSPEAK 4.1. Within each O 1s and V 2p envelopes, the *G/L* ratios of the separate components were constrained to be equal. The derived binding energies (BE) were corrected for the surface charging effect by referencing the adventitious carbon C 1s peak set at 284.5 eV. For comparison, XP spectra of the reference oxides V_2O_5 and α-Al_2O_3 (corundum) were also taken. The areas under the peaks were used to evaluate the surface composition. The relative sensitivity factors were determined from the reference compounds V_2O_5 and Al_2O_3 to be O(1s):V($2p_{3/2}$):Al(2p) = 1:1.91:0.25.

The static ToF-SIMS analysis of the catalysts was carried out with a pulsing (7.7 kHz) beam of 5 keV Ar^+ ions, using a reflectron analyzer. The positive secondary ions extracted at 1,400 V were registered in the mass range up to 400 with a mass resolution of 1,230 at 51 amu. To minimize charging problems during SIMS analysis a special acquisition regime was employed [24]. The XPS and SIMS measurements were performed for each sample in three series and the patterns were found to be reproducible.

3 Results

As an example, Fig. 1a shows the O 1s–V 2p region in XPS spectra of dried and calcined V–Al–O powders precipitated at pH = 5.5 presented on the charge-corrected binding energy scale. One can see that after calcination, the intensity of the O 1s peak in this sample decreases and shifts to lower BE, while the V 2p peak increases in intensity and shifts to higher BE. The appreciable broadening and asymmetry of the O 1s peak in V–Al–O point to a variety of oxygen environments and types of bonds.

We deconvoluted the O 1s spectra, assuming the presence of three configurations for oxygen bonds, O–Al–O

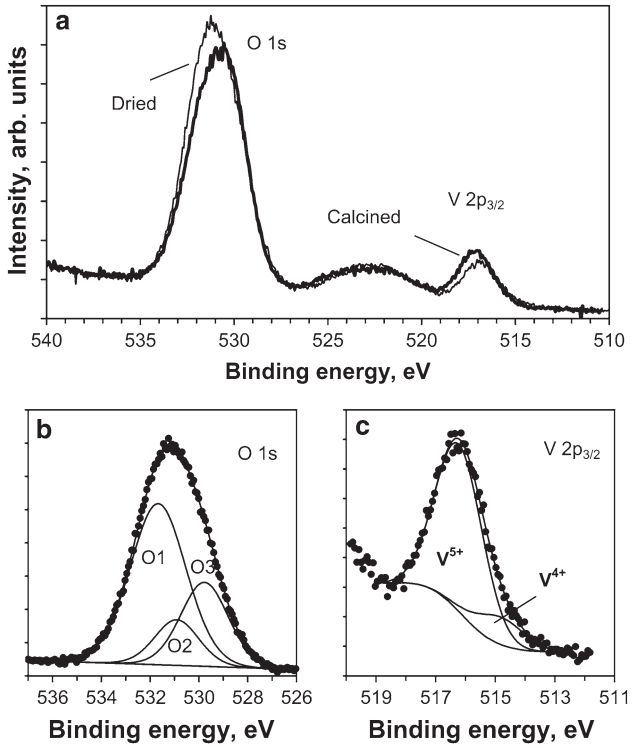

Fig. 1 The O 1s–V 2p X-ray photoelectron spectral region for dried and calcined V–Al–O samples precipitated at pH = 5.5 (**a**) and the results of deconvolution of the O 1s (**b**) and V $2p_{3/2}$ (**c**) lines

(and/or Al–O–H), Al–O–V and O–V–O, represented respectively by components O1, O2 and O3 shown in Fig. 1b. During deconvolution the peak positions and FWHM of the components were allowed to vary freely to attain the best fit. The charge-corrected binding energies of the O1 component were found to vary non-monotonically in the range 531.5–532 eV for dried and 531.4–531.8 eV for calcined catalysts depending on precipitation pH. These values are larger than BE = 530.5 eV (our data, [25]) and 530.7 eV [26] measured for the O^{2-} component in the O 1s spectrum of corundum, but they are close to BE(O1-s) = 531.5 eV [27], 531.65 eV [28] or BE(OH^-) = 531.8 eV [26] in boehmite AlOOH and to BE = 531.44–531.9 eV reported for the OH^- component in the O 1s spectrum of gibbsite and bayerite $Al(OH)_3$ [25–27].

To avoid uncertainty in determining the absolute BE, it is preferable to use the energy separation between the O 1s and Al 2p peaks, ΔBE(O–Al). This parameter is independent of the surface charging and therefore can reliably be applied for the identification of the chemical environment. The energy separations derived from data reported in the literature show that ΔBE(O–Al), on average, increases with the extent of hydroxylation of aluminium. For α-Al_2O_3 (O–Al–O environment), ΔBE(O–Al) is in the range 456.3–456.6 eV ([25, 26, 28]); for boehmite and pseudoboehmite AlOOH (O–Al–OH bonding), ΔBE(O–Al) varies from 456.7 eV [25] to 457.3 eV [26–28], and for $Al(OH)_3$ (Al–OH environment), ΔBE(O–Al) covers the range 457.13–457.7 eV [25–28]. These ranges are shown in Fig. 2a as cross-hatched areas. As can be seen in Fig. 2a, all energy separations ΔBE(O1–Al) for the O1 component in V–Al–O are significantly larger than ΔBE(O–Al) in Al_2O_3 but they fall in the region of the values ΔBE(OH–Al) for hydrated species in trihydroxide $Al(OH)_3$, being also close to ΔBE(O–Al) = 457.3 eV in boehmite AlOOH [26–28]. This means that aluminium on the surface of V–Al–O is largely bonded to hydroxyls (Al–O–H) and forms hydroxide/oxyhydroxide. With an increase in pH, the surface hydroxylation and/or formation of aluminium hydroxide in dried samples appears to slightly grow as indicated by ΔBE(O1–Al) which increases from 457.5 to 457.7 eV (Fig. 2a). In calcined V–Al–O, ΔBE(O1–Al) = 457.3–457.4 eV is practically independent of pH and is close to separations ΔBE(O–Al) in both gibbsite $Al(OH)_3$ [26] and boehmite AlOOH [26–28]. At pH > 5.5, ΔBE(O1–Al) in calcined catalysts is somewhat lower than in dried samples indicating therefore some surface dehydroxylation.

Charge-corrected BE of the O3 component changed non-monotonically in the range 529.9–530.2 eV for dried and 529.6–530.1 eV for calcined V–Al–O that is close to BE = 529.9 eV for O^{2-} species in V_2O_5. On the other hand, the separations ΔBE(O3–V$2p_{3/2}$) point out some differences in the chemical environment of oxygen by V atoms and/or in the vanadium oxidation state in dried and calcined samples. Figure 2b shows that whereas in dried catalysts with increasing pH ΔBE(O3–V$2p_{3/2}$) increases from 12.92 to 13.19 eV, in calcined samples ΔBE(O3–V$2p_{3/2}$) non-monotonically decreases. Besides, calcination causes a noticeable decrease in the ΔBE(O3–V$2p_{3/2}$) values (down to 12.85–12.63 eV), especially at larger pH.

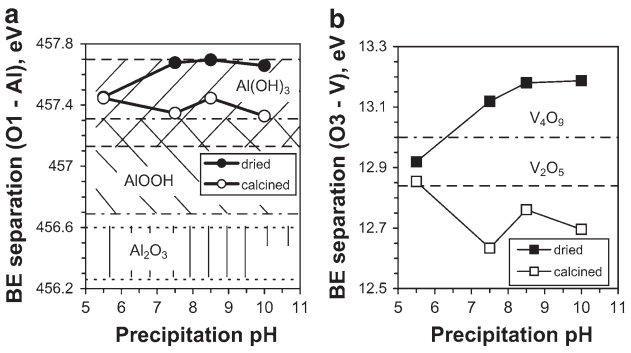

Fig. 2 Binding energy separations between the O 1 and Al 2p peaks (**a**) and between the O3 and V $2p_{3/2}$ peaks (**b**) for dried and calcined V–Al–O catalysts as a function of precipitation pH. According to deconvolution, the O1 and O3 components in the O 1s envelope (see Fig. 1b), represent respectively Al–O and V–O bonds. The *hatched areas* in **a** correspond to ranges of the O1s–Al2p binding energies separations in Al_2O_3, AlOOH and $Al(OH)_3$ reported in the literature

The variations of $\Delta BE(O3–V2p_{3/2})$ in both types of samples are qualitatively similar to those of $\Delta BE(O1–Al)$ (cf. Fig. 2a, b) and thus may imply progressive formation of V–OH bonds in dried V–Al–O and their decomposition upon calcination. Alternatively, since $\Delta BE(O3–V2p_{3/2})$ in calcined samples is close to $\Delta BE(O–V2p_{3/2}) = 12.84$ eV in V_2O_5 this may indicate preferential formation of O–V–O bonds with V^{5+} ions. In dried precursors precipitated at pH > 5.5, $\Delta BE(O3–V2p_{3/2})$ is somewhat larger than $\Delta BE(O–V2p_{3/2}) = 13$ eV reported for V_4O_9 (see Fig. 2b), but appreciably smaller than $\Delta BE = 13.6$ eV in V_6O_{13} [29], and that points to a structural distinction between the O–V–O environments in dried V–Al–O as compared to calcined catalysts and their similarity to O–V bonding in V_4O_9.

The binding energies of the O2 component lying in the range 531–531.4 eV for dried and 530.5–530.7 eV for calcined samples are intermediate between those for the O1 and O3 components and thus may be attributed to the formation of Al–O–V bonds.

Figure 3a shows fractions of the species assigned to O–Al–OH (O1 component), Al–O–V (O2 component) and O–V–O/V–OH bonds (O3 component) in the O 1s spectra of catalysts as a function of pH. The O–Al–OH bonds are predominant in the O 1s envelope; depending on the precipitation pH and treatment conditions their relative fraction, O1/(O1 + O2 + O3), varies from 52 to 60 %. The fractions of the O–V–O and Al–O–V bonds are in the range 27–40 and 8–16 %, respectively. With an increase in the pH, the fractions of the O 1s components vary non-monotonically. In dried samples, a fraction of the O–Al–OH bonds decreases in the range of pH = 5.5–7.5 before increasing at pH > 7.5, whereas a fraction of the O–V–O bonds increases in the range of pH = 5.5–8.5 and drops at pH = 10; a fraction of the Al–O–V bonds non-monotonically decreases and attains a minimum at pH = 8.5. In calcined samples, the O 1s components exhibit opposite trends; namely, the O1 fraction is a maximum and the O3 fraction is a minimum at pH = 7.5, and a fraction of the Al–O–V bonds monotonically increases (Fig. 3a). Calcination of the sample precipitated at pH = 5.5 results in an appreciable increase in the relative abundance of the O–V–O bonds (from 26.6 to 34.1 %) and in a decrease in the fraction of the O–Al–OH and Al–O–V bonds so that the ratio of the oxygen components O3/O1 increases from 0.44 to 0.62. With an increase in the pH, the O3/O1 ratio varies similarly to the O–V–O fraction, displaying a non-monotonic increase for dried catalysts (with a maximum at pH = 8.5) and a decrease for calcined catalysts (with a minimum at pH = 7.5). Accordingly, at pH > 5.5 the O3/O1 ratio in dried V–Al–O is noticeably larger than that in calcined samples.

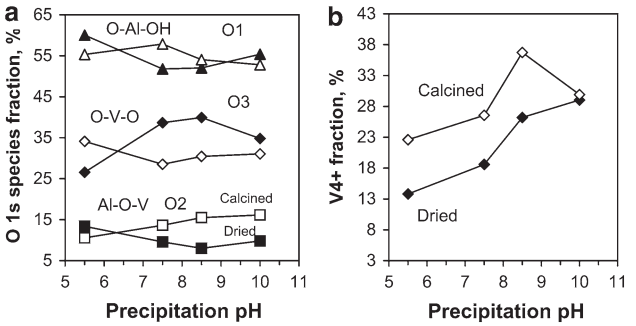

Fig. 3 Fractions of the O1, O2 and O3 components in the O 1s envelope assigned, respectively to O–Al–OH, Al–O–V and O–V–O bonds (**a**) and fraction of the reduced V^{4+} species in the V $2p_{3/2}$ envelope (**b**) of dried (*filled symbols*) and calcined (*open symbols*) catalysts as a function of pH

The O1 component in the O 1s spectrum has the largest FWHM indicating the presence of several oxygen–aluminium environments and an influence of the structural variety (such as Al–OH bonds in AlOOH or $Al(OH)_3$ gibbsite and bayerite). In dried V–Al–O, the O1 FWHM is about 2.7 eV, whereas in calcined samples the O1 FWHM varies in the range 2.7–3.1 eV so as to form a maximum at pH = 8.5. The FWHM of O3 (O–V–O and O–V–OH bonds) is smaller than that of O1 and is about 2.2–2.3 eV. In calcined catalysts, the O3 FWHM, like the O1 FWHM, is a maximum at pH = 8.5. The O2 FWHM (Al–O–V bonds) in both dried and calcined catalysts changes between 1.9 and 2.3 eV.

Variations of FWHM of the whole O 1s peak and of the Al 2p and V $2p_{3/2}$ peaks in dried and calcined catalysts as a function of pH are shown in Fig. 4a, b. In both dried and calcined samples, the O 1s peak is the widest (FWHM = 3.3–3.5 eV); the Al 2p and V $2p_{3/2}$ peaks are appreciably narrower and their FWHM are close. With an increase in pH the FWHM of all the peaks varies in the same way. In dried samples, the largest FWHM of the peaks is observed at pH = 7.5, whereas in calcined catalysts the widest peaks of the components of V–Al–O

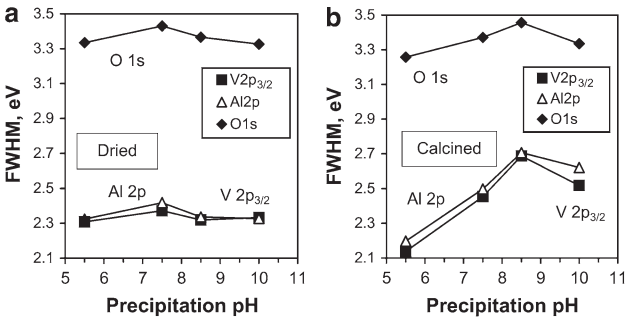

Fig. 4 FWHM of the O 1s, Al 2p and V $2p_{3/2}$ photoelectron peaks in dried (**a**) and calcined (**b**) catalysts as a function of pH

correspond to pH = 8.5. After calcination of V–Al–O precipitated at pH > 5.5 the FWHM of the Al 2p and V $2p_{3/2}$ peaks becomes larger than that in dried samples (Fig. 4a, b).

The V $2p_{3/2}$ peak in V–Al–O catalysts with a FWHM of 2.31–2.37 eV for dried and 2.23–2.69 eV for calcined samples happens to be rather broad as compared with V_2O_5 (FWHM = 1.43 eV) which indicates the presence of vanadium in several oxidation states. We deconvoluted the V $2p_{3/2}$ lines by using two components representing the vanadium species in different charge states (Fig. 1c); the FWHM of the components were constrained to be equal. A dominant component in the V $2p_{3/2}$ envelope of the catalysts with a FWHM of 1.6–1.8 eV arose at BE = 516.8–517.1 eV, which corresponds to the position of the V $2p_{3/2}$ peak in the reference oxide V_2O_5 (BE = 517.0 eV) and is related to the V^{5+} oxidation state. The other component was found to be shifted by 1.2–1.5 eV to lower BE (Fig. 1c) and could be assigned to the V^{4+} state [29, 30]. In dried V–Al–O, the derived fraction of reduced V^{4+} species in the V $2p_{3/2}$ envelope, $V^{4+}/(V^{4+}+V^{5+})$, rose monotonically with increasing pH and varied in the range 13.8–29 %. Calcination caused an increase in the abundance of the V^{4+} species in the catalysts; with an increase in pH, the V^{4+} fraction increased from 22.6 to 36.7 % and demonstrated a maximum at pH = 8.5 before decreasing to 29.9 % at pH = 10 (Fig. 3b). Note that the energy separation between the V^{5+} and V^{4+} components in calcined samples was also a maximum (~1.4 eV) at pH = 8.5 possibly indicating the additional presence in this catalyst of some amount of the V^{3+} state.

After calcination of the sample precipitated at pH = 5.5 the V $2p_{3/2}$ peak shifted by 0.26 eV to higher BE and the O 1s peak moved by 0.15 eV to lower BE, whereas the Al 2p BE remained practically unchanged. This fact implies that calcination of V–Al–O at pH = 5.5 caused an increase in ionicity of the V–O bonds. Besides, the O 1s charge-corrected binding energy in calcined samples turned out to be less than that in dried V–Al–O whatever the pH, thus indicating that after calcination oxygen in the catalyst became more negatively charged.

Variations of the V $2p_{3/2}$, Al 2p and O 1s charge-corrected binding energies in calcined catalysts precipitated at different pH are presented in Fig. 5a as BE shifts in reference to the respective values in the calcined sample precipitated at pH = 5.5. As can be seen in Fig. 5a, by increasing the pH up to 8.5 all the peaks in calcined V–Al–O shift progressively to lower BE before shifting back at pH = 10, thus exhibiting a deep minimum in BE at pH = 8.5. This trend is different from variations of the V $2p_{3/2}$, Al 2p and O 1s BE as a function of pH for dried catalysts [17] which demonstrated a maximum in BE for the sample precipitated at pH = 7.5. Note that variations of BE of the V $2p_{3/2}$, Al 2p and O 1s peaks closely correlate with variations of their FWHM. However, while in dried samples the correlation is direct and the largest positive shift of BE observed at pH = 7.5 (Fig. 3 in [17]) corresponds to the largest FWHM (Fig. 4a), in calcined V–Al–O the correlation is inverse and the largest negative shift of BE corresponds to a maximum broadening of the peaks at pH = 8.5 (cf. Figs. 4b, 5a).

The correlated change of binding energies of the V $2p_{3/2}$, Al 2p and O 1s peaks and their FWHM (Figs. 4b, 5a) and also of FWHM of the O–Al–OH and O–V–O components of the O 1s peak in calcined V–Al–O as a function of pH indicates alterations in the chemical and structural state of the samples caused by changing the precipitation conditions. The increasing non-monotonic broadening of the peaks that occurs with an increasing precipitation pH can be associated with increasing diversification of local atomic environments. Thus, the local environments Al–O–Al and V–O–V in calcined V–Al–O appear to be modified by increasing the fraction of the Al–O–V bonds (see

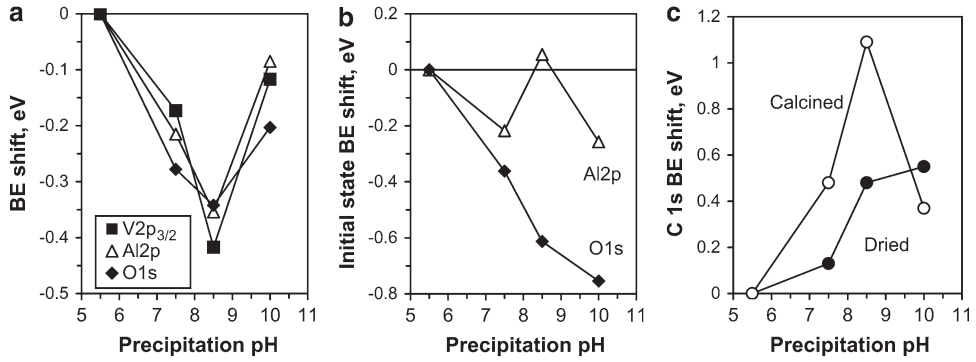

Fig. 5 **a** Variations of the V $2p_{3/2}$, Al 2p and O 1s binding energies in calcined V–Al–O as a function of precipitation pH in reference to the sample precipitated at pH = 5.5; **b** the shifts of the Al 2p and O 1s binding energies in calcined V–Al–O caused by the initial state effects ($\Delta E_b(\mathrm{ISE}) = k\Delta q + \Delta V_M$); **c** the shift of the C 1s line with respect to C 1s BE at pH = 5.5 in dried and calcined V–Al–O as a function of pH

Fig. 3a) and varying the extent of hydroxylation (Fig. 2a). The inverse variations of the V $2p_{3/2}$ BE and FWHM can largely be associated with the correlated variation of the V^{4+} fraction in calcined catalysts (see Fig. 3b).

In general terms, the change in BE of the XPS peak of a given element A in two different materials (BE shift) can be written as [31].

$$\Delta E_b^A = k\Delta q^A + \Delta V_M^A - \Delta R_{ea}^A \quad (1)$$

where q^A is the local valence charge on the atom A, $V_M^A = \Sigma q^B / r^{A-B}$ is the Madelung energy, q^B are the net charges of all other atoms in the compound, r^{A-B} are their distances from the core-ionized atom, and R_{ea}^A is the extra-atomic part of the relaxation energy. The contribution $k\Delta q^A + \Delta V_M^A$ to the measured BE shift arises from the initial state effects (ISE) and reflects the change in the initial state chemistry. The change of the extra-atomic relaxation energy can be evaluated through the change of the Auger parameter as $\Delta R_{ea}^A = \Delta\alpha'_A/2$.

The modified Auger parameter $\alpha'(A)$ is defined as a sum of binding energy of particular photoelectrons ejected from element A and kinetic energy (KE) of X-ray excited Auger electrons emitted from this element. Auger parameters, being unsusceptible to charging effects, are therefore particularly useful in characterizing the electronic properties of oxides [31]. X-ray induced Auger spectra measured for O, V and Al in previous work [17] were used to determine the Auger parameters and BE shifts brought about by the initial state effects alone in dried V–Al–O catalysts. In this work we determined the Auger parameters for oxygen $\alpha'(O) = BE(O\ \ 1s) + KE(O\ \ KL_{23}L_{23})$ and aluminium $\alpha'(Al) = BE(Al\ 2p) + KE(Al\ KLL)$ in calcined catalysts and thus derived the BE shifts $\Delta E_b^A(ISE) = k\Delta q^A + \Delta V_M^A$ caused entirely by variation of the atomic charge and Madelung energy. Such BE shifts for the O 1s and Al 2p peaks in calcined V–Al–O precipitated at different pH are presented in Fig. 5b. The Auger parameters for vanadium were not evaluated because of a large error in determining the energy position of the smeared V LMM Auger peaks.

It can be seen that, in contrast to measured BE, the variation of the BE related to the ISE is different for different peaks (cf. Fig. 5a, b). The ISE BE of the O 1s photoelectrons monotonically decreases with an increasing pH, with the negative shifts ΔBE_{ISE} with respect to BE at pH = 5.5 being larger than the corresponding shifts ΔBE_{meas} for all pH ≠ 5.5. The largest difference between ΔBE_{ISE} and ΔBE_{meas} is observed at pH = 10 (−0.75 and −0.2 eV, respectively). The increasing difference between the O 1s BE shifts ΔBE_{ISE} and ΔBE_{meas} at high pH (>7.5) in calcined V–Al–O results from the drop in the extra-atomic relaxation energy caused by a decrease in the polarizability of oxygen atoms, which may be associated with an alteration in the prevailing oxygen environments, for example, from O–Al–OH to O–V–O and Al–O–V (see Fig. 3a). The progressive shift of the O 1s peak to lower BE with increasing pH implies the rise of the negative partial charge on oxygen atoms in V–Al–O and can be related to increasing oxygen nucleophilicity (bond ionicity), which was suggested to be an important factor in the enhancement of the catalytic activity (propene formation rate) of dried V–Al–O [17].

The shift of the Al 2p ISE BE also has a non-monotonic character with a maximum at pH = 8.5 but lies in a narrower region from 0 to −0.26 eV. Note the close qualitative similarity between variations of the ΔBE_{ISE} (Al2p) and ΔBE(O1–Al) in calcined V–Al–O as a function of pH (cf. Figs. 2a, 5b) which implies that they are caused by changes in the extent of hydroxylation of the catalyst.

The variation of the carbon peak BE in dried and calcined V–Al–O versus pH is plotted in Fig. 5c as a shift of the C 1s line with respect to C 1s BE at pH = 5.5. It can be seen that the shift of the C 1s peak in the catalysts, which typically reflects surface charging during XPS analysis, strikingly resembles the variations of the V^{4+} fraction in the dried and calcined samples (cf. Figs. 3b, 5c). In calcined V–Al–O, the C 1s BE shift exhibits a maximum at pH = 8.5 and is also qualitatively very similar to the behavior of FWHM of the O 1s, Al 2p and V $2p_{3/2}$ peaks in these samples (cf. Figs. 4b, 5c). Indeed, surface charging can result in respective broadening of XPS peaks. On the other hand, surface charging depends on the composition and structure of an insulator. The observed variations of surface charging in calcined V–Al–O seem to reflect chemical and structural transformations and imply formation at pH = 8.5 of a structure with the highest content of a dielectric phase.

According to the results of a quantitative analysis, the surface atomic composition of V–Al–O at pH = 5.5 corresponds to 5 at.% V–25.2 at.% Al–69.8 at.% O (VAl_5O_{14}) in the dried catalyst and 6.4 at.% V–26.8 at.% Al–66.8 at.% O ($VAl_{4.2}O_{10.4}$) in the calcined sample. At pH = 10 it changes to 2.3 at.% V–29.9 at.% Al–67.8 at.% O ($VAl_{12.9}O_{29.2}$) and 3.2 at.% V–32.8 at.% Al–64 at.% O ($VAl_{10.3}O_{20}$) in the dried and calcined samples, respectively. Figure 6a, b, and c show that the surface concentrations of V, Al and O in the catalyst vary monotonically as a function of precipitation pH, with the trends being very similar for dried and calcined samples. It is seen that an increase in precipitation pH gives rise to a decrease in the vanadium and oxygen content and to an increase in the aluminium surface concentration. On the other hand, calcination results in an enrichment of the surface with V and Al and in a depletion of oxygen for all the samples precipitated at any pH. The V/Al atomic ratio on the surface of V–Al–O drops in dried and calcined catalysts, respectively from ∼0.2 to 0.07 and from 0.24 to 0.1 as the pH grows

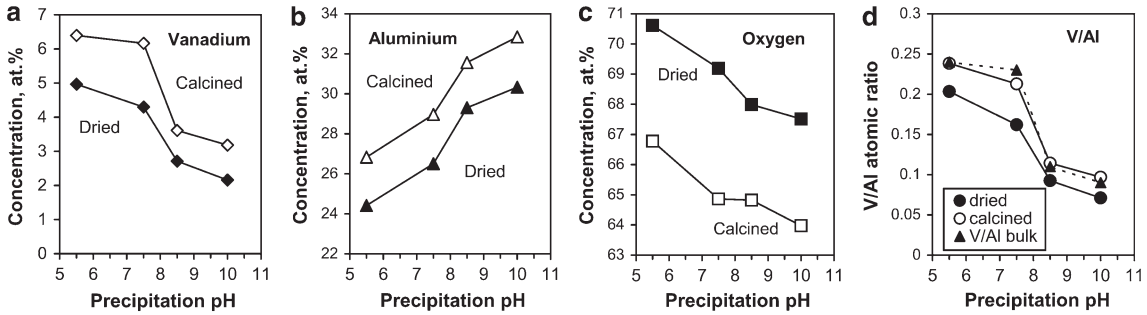

Fig. 6 Variations of the XPS-derived surface concentration of V (**a**), Al (**b**), O (**c**) and of the V/Al atomic ratio (**d**) in dried and calcined V–Al–O as a function of pH

(Fig. 6d). Comparison of the V/Al ratios for the surface and the bulk (determined by inductively coupled plasma atomic emission spectroscopy [16]) shows that the surface of dried catalysts is depleted of vanadium in comparison with the bulk; however, after calcination this depletion nearly vanishes (especially at higher pH), and the surface V/Al atomic ratio in calcined catalysts approaches the bulk one (Fig. 6d). Note that while the vanadium surface concentration decreases with an increasing pH, the abundance of the reduced V^{4+} species in V–Al–O increases (Fig. 3b). A similar effect was observed for supported V_2O_5/TiO_2–Al_2O_3 [32] and V_2O_5/ZrO_2 catalysts [7] in which the fraction of V^{4+} species decreased with an increase in the V_2O_5 loading.

Figure 7 shows XPS valence band spectra of dried and calcined V–Al–O catalysts precipitated at pH = 10 and of the reference oxide Al_2O_3. The valence band structure of V–Al–O differs from that of Al_2O_3 and V_2O_5 (shown in [17]) though some contributions from both oxides can be implicated. In V_2O_5, which has an empty 3d-shell, the valence band is mainly composed of the O 2p states that are hybridized with the V 3p states [33, 34]. In Al_2O_3, the broad region is due to the O 2p states with some Al 3s and Al 3p character [25, 33]. In V–Al–O, the spectrum demonstrates a band gap of about 2.2–3 eV and a filled region with a maximum at ~5.9–7 eV. As the pH is increased the onset of the valence band shifts to higher binding energies, indicating a decrease in the degree of ionicity experienced by the oxygen in the valence band and, respectively, the enhancement of dielectric properties of V–Al–O. The valence band in V–Al–O is noticeably broader (~13 eV) than that in Al_2O_3 (~9.6 eV) and V_2O_5 (~7.3 eV) and, being largely of O 2p character, may also involve the V 3p and Al 3p states. Indeed, the difference spectrum obtained by subtracting the valence band of the dried catalyst from that of calcined V–Al–O at pH = 10 (Fig. 7, curve 4) implies that the enhancement of intensity occurring in the region ~4.9–11.4 eV as a result of calcination may be caused by an increase in the surface concentration of V and Al (see Fig. 6a, b). Note that with an increasing pH the shape of the valence band of calcined V–Al–O changes to some extent. The difference spectrum obtained by subtracting the valence band of the calcined catalyst precipitated at pH = 5.5 from that precipitated at pH = 10 (Fig. 7, curve 5) exhibits some enhancement of the emission intensity in the band region ~7.6–12.8 eV, which corresponds to the region of maximum intensity in the Al_2O_3 spectrum (curve 3). This may be associated with the growing contribution of the alumina-related states and Al–O bonds to the valence band of V–Al–O. Thus the changes in the valence band reflect alterations in the surface chemical composition and structure of V–Al–O caused by varying precipitation conditions and heat treatment.

The SIMS spectra obtained by Ar^+ bombardment of V–Al–O contain a set of peaks of atomic and molecular secondary ions related to the main components. The V^+/Al^+ ion intensity ratio in V–Al–O monotonically decreases

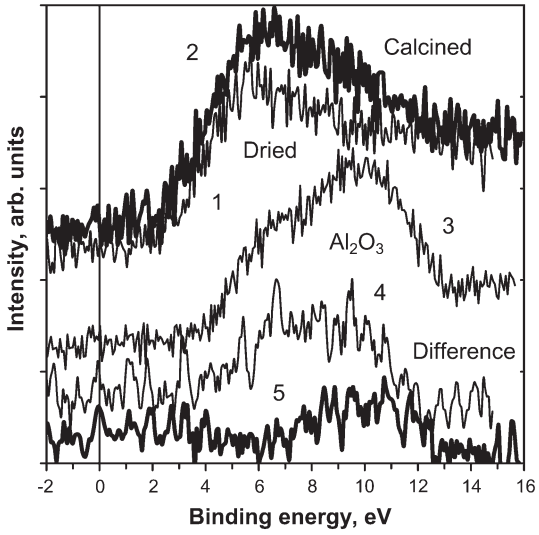

Fig. 7 Valence band spectra of dried (*1*) and calcined (*2*) V–Al–O catalysts precipitated at pH = 10 and of the reference oxide Al_2O_3 (*3*). The difference spectra obtained by subtracting the valence band of dried catalyst from that of calcined V–Al–O at pH = 10 (*4*) and by subtracting the valence band of calcined catalyst precipitated at pH = 5.5 from that precipitated at pH = 10 (*5*) are also shown

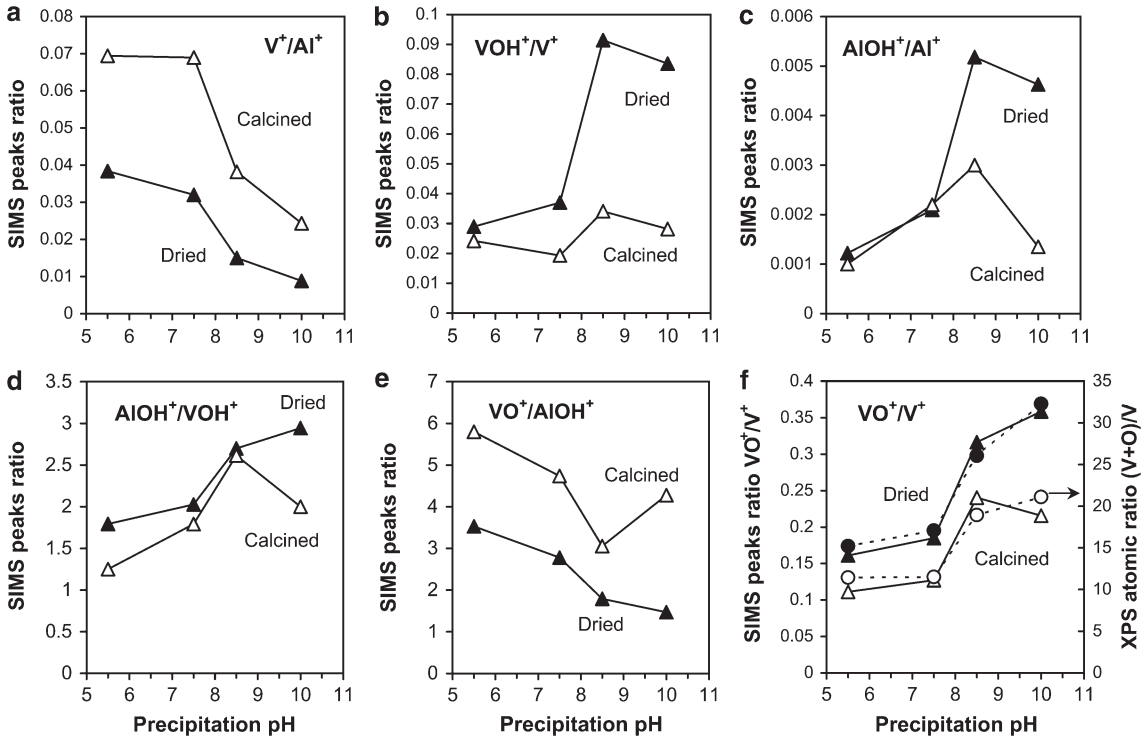

Fig. 8 Variations of the V^+/Al^+ (**a**), VOH^+/V^+ (**b**), $AlOH^+/Al^+$ (**c**), $AlOH^+/VOH^+$ (**d**), $VO^+/AlOH^+$ (**e**) and VO^+/V^+ (**f**) SIMS ion peaks ratios in dried and calcined V–Al–O as a function of pH. For comparison, in **f** are also shown the XPS (V + O)/V atomic ratios

with increasing pH (Fig. 8a), indicating a progressive depletion of the catalyst surface of vanadium and/or enrichment in aluminium. After calcination the V^+/Al^+ ratio increases for all pH. Since the heat treatment resulted in increasing the surface concentration of both V and Al (Fig. 6a, b) the enhanced V^+/Al^+ ratios in the calcined samples point to a prevailing enrichment of the surface with vanadium. Note a remarkable correlation between the variations of the SIMS V^+/Al^+ ratio, those of the XPS-derived surface vanadium concentration and the V/Al atomic ratio for dried and calcined catalysts (cf. Figs. 6a, d, 8a).

Variations of the VOH^+/V^+ and $AlOH^+/Al^+$ ion peaks ratios as a function of pH (Fig. 8b, c) in dried V–Al–O catalysts indicate an enhanced formation at higher pH of hydroxylated vanadium species (V–OH bonds) and aluminium hydroxides/oxyhydroxides. Calcination of the precursor reduces the extent of hydroxylation, especially at pH > 7.5. In calcined samples, hydroxylation of vanadium remains low and practically independent of pH (Fig. 8b); hydroxylation of aluminium attains a maximum at pH = 8.5 but is still significantly lower than that in the dried counterpart (Fig. 8c). Note the similarity of variations of the VOH^+/V^+ and $AlOH^+/Al^+$ ion peaks ratios in dried and calcined samples and variations of the energy separation ΔBE(O1–Al) in XPS indicating the extent of aluminium hydroxylation (cf. Figs. 2a, 8b, c).

With an increasing pH, formation of aluminium hydroxides/oxyhydroxides in the catalysts appears to prevail over vanadium hydroxylation, which is indicated by the growth of the ion peaks ratio $AlOH^+/VOH^+$ (Fig. 8d). In calcined catalysts, the $AlOH^+/VOH^+$ ratio is less than that in dried V–Al–O due to a smaller extent of aluminium hydroxylation and exhibits a maximum at pH = 8.5. Note that variations of the SIMS $AlOH^+/VOH^+$ ratio in both dried and calcined catalysts are similar to variations of the XPS C 1s peak BE (cf. Figs. 5c, 8d), which are associated with the surface charging and thus can be caused by varying the amount of the dielectric phase AlOOH/$Al(OH)_3$ in V–Al–O.

The $VO^+/AlOH^+$ ion peaks ratio in dried catalysts monotonically decreases with increasing pH, whereas in calcined V–Al–O it attains a minimum at pH = 8.5 (Fig. 8e). After calcination the $VO^+/AlOH^+$ ratio increases and becomes larger than that in the dried samples, whatever the pH. At the same time, the VO^+/V^+ ratio demonstrates just the opposite behaviour as compared to the $VO^+/AlOH^+$ ratio: it monotonically increases in dried V–Al–O and attains a maximum at pH = 8.5 in calcined catalysts; besides, after calcination this ratio becomes less than that before calcination (Fig. 8f). Note that variations of the SIMS VO^+/V^+ ratio in dried and calcined catalysts are very similar to variations of the XPS (V + O)/V atomic ratio (Fig. 8f, dashed lines). This means that the VO^+/V^+

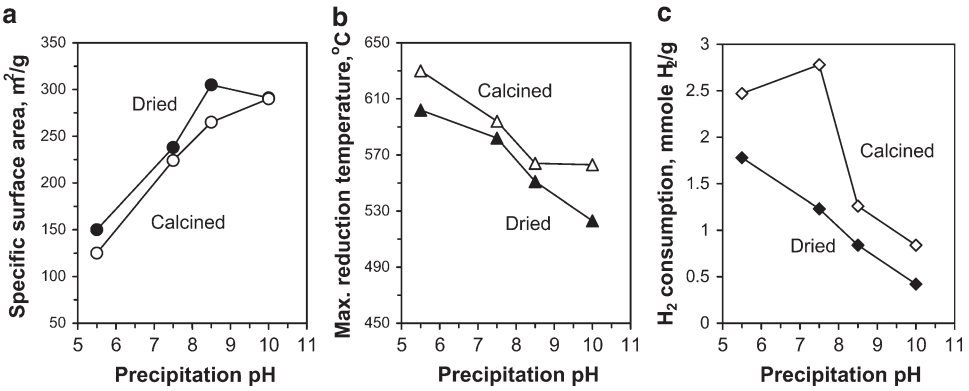

Fig. 9 Variations of the specific surface area (**a**), maximum temperature of reduction (**b**) and hydrogen consumption (**c**) in dried and calcined V–Al–O as a function of pH

ratio is dominated by variations of the oxygen and vanadium surface concentrations. After calcination the surface concentration of vanadium increases whereas the total amount of oxygen decreases (Fig. 6a, c) which leads to a decrease in the (V + O)/V atomic ratio and VO^+/V^+ ion ratio.

For both dried and calcined catalysts, the specific surface area gradually increases as the precipitation pH increases (Fig. 9a). Calcination of the solids caused a significant decrease in the surface area, with the exception of the catalyst obtained at pH = 10 for which practically no change was observed.

As can be seen in Fig. 9, reducibility of the catalysts (b) and consumption of hydrogen (c) depend strongly on the precipitation pH and the thermal treatment of the samples. Both maximum reduction temperature and H_2 consumption per gram of catalyst decrease noticeably with an increasing precipitation pH. After calcination, the maximum reduction temperature and H_2 consumption become larger than in dried samples, whatever the pH.

We have found that the above physico-chemical characteristics of V–Al–O (Fig. 9), being modified by both precipitation pH and heat treatment, exhibit a good general correlation with the surface vanadium concentration. So, Fig. 10 shows that increasing the surface vanadium concentration (induced by decreasing precipitation pH and calcination) is accompanied by a decrease in the specific surface area (a) and by an increase in the maximum temperature of reduction (b) and H_2 consumption (c) in both dried and calcined catalysts. A similar decrease in the specific surface area was typically observed in vanadium oxide catalysts supported on alumina [35, 36], prepared by incipient wetness, with an increase in vanadia loading or surface vanadium (VO_x) density. In TiO_2/SiO_2-supported vanadia catalysts obtained by impregnation, both the surface area and reducibility were also observed to decrease with increasing vanadia loading (V surface density) [8].

Finally, Fig. 11 presents the results of the catalytic activity tests in the propane ODH reaction for the V–Al–O powders. Since the vanadium concentration in the catalyst varies as a function of pH, the catalytic activity is expressed in terms of the number of moles of converted propane or moles of produced propene per hour and per gram-atom of vanadium. It can be seen that the rates of propane conversion (Fig. 11a) and propene production (Fig. 11b) exhibit a slight augmentation in the range of pH = 5.5–7.5 followed by a fast increase at pH > 7.5. The calcination of the V–Al–O precursors improves their catalytic properties whatever the pH.

Figure 11c shows the propene formation rates for the various V–Al–O catalysts as a function of propane conversion rates. It can be seen that there is a clear linear correlation with a slope of the line of about 0.42. This means that the propene selectivity is practically constant

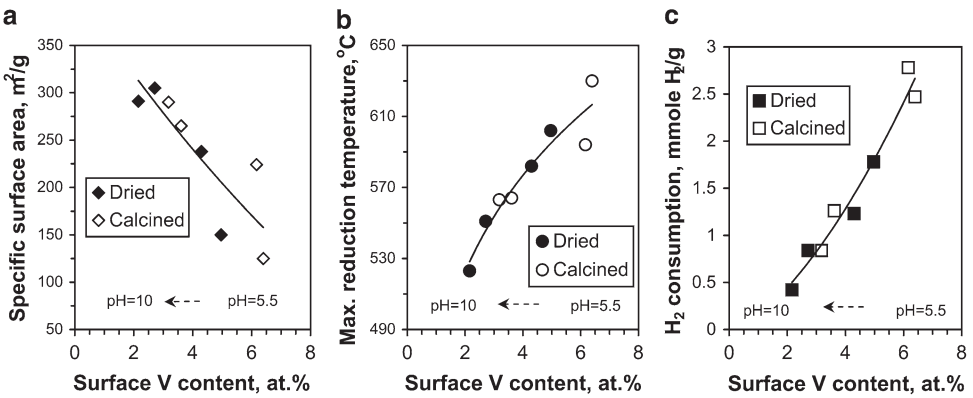

Fig. 10 Dependence of the specific surface area (**a**), maximum temperature of reduction (**b**) and hydrogen consumption (**c**) on the surface vanadium content in dried and calcined V–Al–O

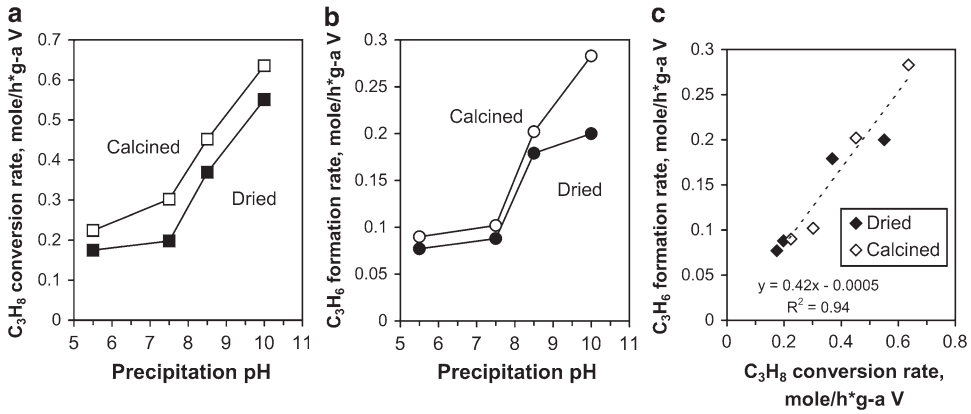

Fig. 11 Variations of the propane conversion rate (**a**) and propene formation rate (**b**) in dried and calcined V–Al–O as a function of pH. In **c**, the correlation between the propane conversion rate and propene productivity is shown for all catalysts

(∼42 % on the average) for all catalysts no matter if dried or calcined, no matter which pH. In other words, the 'loss' or selectivity to CO and CO_2 is also constant, so that CO and CO_2 competitive formation remains unchanged. This is quite remarkable, because despite the fact that each point in Fig. 11c corresponds to a different catalyst, i.e. the data include catalysts that were precipitated at different pH, with different heat treatments, the intrinsic surface chemistry seems to be identical. This strongly suggests that either propane ODH is insensitive to the surface structure of the catalyst or that under reaction conditions all the catalysts have nearly identical surface structures. The latter possibility would imply a quasi-equilibrium between the catalyst phases and the existence of only one type of catalytically active site (or ensemble of surface atoms).

4 Discussion

The results described above demonstrate the reliability and power of a combined analysis by XPS and SIMS so as to relate the physico-chemical properties and the catalytic performance of catalysts, in general, and V–Al–O, in particular. Variations in the specific preparation conditions of V–Al–O as, for example, acid–base settings, drying and calcinations have been shown to cause appreciable changes in these properties/performances. More specifically, increasing the precipitation pH of the aqueous solution gives rise to the development of the specific surface area, the progressive depletion of the catalyst surface of oxygen and vanadium and the enrichment with aluminium, the lowering of the maximum reduction temperature and hydrogen consumption, and, finally, to the improvement of catalytic properties. The major oxidation state of vanadium in V–Al–O is +5, although an appreciable fraction of reduced V^{4+} species is also present at the surface. With an increasing pH the abundance of the V^{4+} ions in the catalysts increases and, accordingly, the average oxidation state of vanadium decreases from ca. +4.86 to +4.71 in the dried catalysts and from ca. +4.77 to +4.63 in the calcined ones. Aluminium in V–Al–O is largely terminated by hydroxide/oxyhydroxide. As the pH grows, the extent of Al hydration and the amount of Al hydroxide non-monotonically increases. Vanadium is also hydroxylated to some extent, though much less than aluminium.

The calcination in air at 500 °C brings about significant alterations in the physico-chemical state of the catalyst. At any pH, the surface area and reducibility of V–Al–O decrease, the hydrogen consumption increases, the surface concentration of V and Al increases (so that the V/Al atomic ratios approach the bulk values) and that of oxygen decreases. After calcination the relative fraction of reduced V^{4+} species in V–Al–O increases, the extent of hydroxylation of Al and V decreases, $Al(OH)_3$ transforms largely into AlOOH, and Al–O and V–O bond strengths change, giving rise to modification of the valence band electronic structure. The calcination favors solid state reactions to form strong, more thermodynamically stable interactions between the metal oxides or the separated structures of vanadium and aluminum, leading to an increasing abundance of the Al–O–V bonds with increasing pH. As a consequence of these chemical and structural alterations (and despite the deterioration of reducibility) the catalytic activity of the calcined V–Al–O increases.

Taking into account that the calcination was performed in air, under oxidizing conditions, a significant loss of oxygen in V–Al–O catalysts precipitated at any pH after heat treatment (Fig. 6c) appears unexpected. The surface dehydroxylation caused by calcination may partly be responsible for the observed diminution of the oxygen content. However, the main reason for the decrease in the surface oxygen concentration in calcined samples as compared to dried V–Al–O appears to be the reduction of vanadium oxide during heat treatment which is supported by an increased abundance of reduced V^{4+} species in calcined powders (Fig. 3b). A similar effect was observed in $VOPO_4/TiO_2$ and $VOPO_4/Al_2O_3$ catalysts which demonstrated an increase in the abundance of reduced V^{4+}

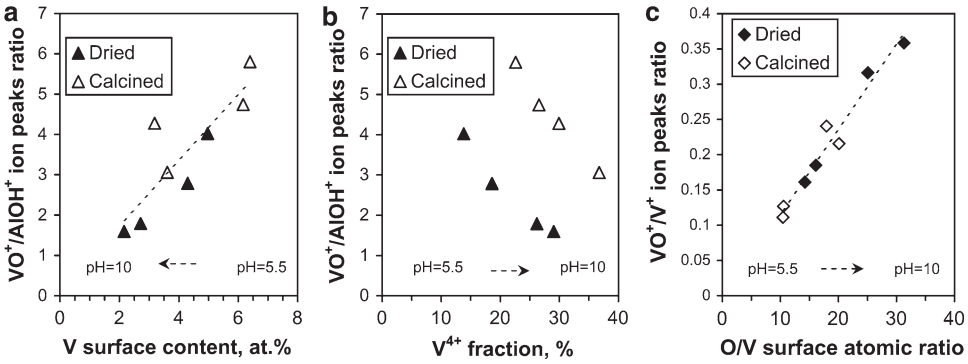

Fig. 12 Correlations between the XPS-derived V surface concentration and the SIMS-derived $VO^+/AlOH^+$ ion peaks ratio (**a**), between fraction of reduced V^{4+} species and $VO^+/AlOH^+$ ratio (**b**) and between O/V surface atomic ratio and VO^+/V^+ ion peaks ratio in dried and calcined V–Al–O

species revealed by XPS after calcination of dried (80 °C) precursors in air at 450, 550 and 650 °C for 3 h [13]. The presence of an appreciable fraction of the V^{4+} species in the supported catalysts calcined at 500–650 °C in air was also reported for the $V_2O_5/TiO_2–Al_2O_3$ [32], V_2O_5/ZrO_2 [7] and V_2O_5/SiO_2, $V_2O_5/TiO_2–SiO_2$ [37] systems; the reasons for such reduction of vanadium during heat treatment under aerobic conditions, however, are still unclear.

We believe that the $VO^+/AlOH^+$ SIMS ratio may characterize coverage of the aluminium hydroxide/oxyhydroxide support by vanadium oxide particles and, respectively, their dispersion. In V–Al–O, vanadium forms dispersed oxides, and no crystalline V_2O_5 is detected. According to a Raman spectroscopy study of dried V–Al–O, the catalyst structure may be assumed to be a polymer linking of tetrahedral $[VO_x]_n^{n-}$ units [16] which are supported on Al hydroxide/oxyhydroxide. A decrease in the $VO^+/AlOH^+$ ratio observed in dried V–Al–O with an increasing pH (Fig. 8e) may thus reflect the decreasing extent of polymerization (decreasing coverage of the support) and is in accordance with a reduction of the intensity of bands corresponding to the $[VO_x]_n^{n-}$ polymeric vanadium species in Raman spectra [16] and with a decrease in the surface concentration of vanadium (Fig. 6a). After calcination, vanadium and aluminium contents at the surface increase, with the V concentration rising stronger. Accordingly, at any pH the V/Al atomic ratio and the $VO^+/AlOH^+$ ion ratio in calcined samples become larger than in the respective dried catalysts (Figs. 6d, 8e). As can be seen in Fig. 12a, this general trend manifests itself in a linear correlation between the $VO^+/AlOH^+$ ion ratio and the surface V concentration (or V/O, V/(Al + O) surface atomic ratios) for both types of the samples. An additional contribution to the enhancement of the $VO^+/AlOH^+$ ratio for calcined catalysts may result from the different chemical and structural state of aluminium in dried and calcined V–Al–O. In the calcined catalysts, aluminium is less hydroxylated and is close to the AlOOH oxyhydroxide state (Fig. 2a), from which the probability of emission of $AlOH^+$ ions should be less than from $Al(OH)_3$. This factor may also be responsible for a deep minimum in the $VO^+/AlOH^+$ ratio for calcined sample at pH = 8.5, for which the extent of hydroxylation [with possible transformation into $Al(OH)_3$] attains a maximum (Figs. 2a, 8c). The sensitivity of emission of the $AlOH^+$ ions to the structural state of the support results in a large scatter of the data points in the correlation plot (Fig. 12a).

Note also an inverse correlation between the $VO^+/AlOH^+$ ion ratio and the fraction of reduced V^{4+} species in dried and calcined catalysts (Fig. 12b). It indicates that the emission of VO^+ molecular secondary ions is sensitive to the presence of reduced vanadium and decreases with an increasing amount of oxygen vacancies (or with a decreasing abundance of the V–O bonds). The fact that the increase in the V^{4+} fraction comes along with a decrease in the surface V concentration implies that more dispersed vanadium oxide phases, which have a higher surface to bulk ratio, could experience more facile reduction during treatments.

The VO^+/V^+ ion ratio also depends on the vanadium surface concentration, but this dependence is inverse (hyperbolic). When plotting the VO^+/V^+ ratio versus O/V atomic ratio, an excellent linear correlation is obtained (Fig. 12c). This correlation implies that the VO^+/V^+ ratio is sensitive to a local coordination environment of V atoms with O atoms in the supported VO_x species and is insensitive to the structural state of the support. The variation of the VO^+/V^+ ratio as a function of pH (Fig. 8f) thus indicates structural modification of vanadium species in the samples. At pH between 5.5 and 7.5, precipitation of metavanadates VO_3^- and polyvanadates $V_4O_{12}^{4-}$ and $V_3O_9^{3-}$ existing in the solution produces tetrahedral polymeric $[VO_3]_n^{n-}$ species adsorbed on aluminum hydroxide. The solid obtained at pH = 8.5 seems to be formed by adsorption of divanadates $V_2O_6(OH)^{3-}$, $V_2O_7^{4-}$ which are the predominant species in the solution. At pH = 10, the presence of isolated monovanadate tetrahedral vanadium species $[VO_4]^{3-}$ or short-chain $[VO_4]_n^{n-}$ species connected to the support via V–O–Al bonds may be assumed. Calcination of the samples precipitated at pH 5.5–7.5 brings about a noticeable increase in the V surface concentration and a decrease in the O concentration

(Fig. 6a, c), and, according to Raman spectroscopic data [16], polymerized $[VO_3]_n^{n-}$ species are largely transformed into octahedral decavanadate species $[V_{10}O_{28-x}]$. However, after calcination of the catalysts prepared at pH $\geq$ 8.5, the $[VO_3]_n^{n-}$ species in a polymerized state again dominate, as indicated by the Raman spectra.

Such structural transformations occurring with an increase in pH and under heat treatment, which are accompanied by changes in coordination of the V atom with oxygen atoms (changes of the O/V atomic ratio in the VO_x unit), can result in a consistent increase of the VO^+/V^+ ratio in dried and calcined samples and in a decrease in the VO^+/V^+ ratio after calcination. Accordingly, variations in the state of coordination and degree of polymerization of the vanadium species and of their interaction with the support can modify the reducibility pattern and result in the variation of binding energies and FWHM of the XPS core-level lines.

Both XPS- and SIMS-derived characteristics turned out to be very sensitive to changes in the physico-chemical state of the catalyst surface induced by chosen precipitation pH and calcination. Interestingly, calcined V–Al–O precipitated at pH = 8.5 stands out and shows particular characteristics. Obviously, under such conditions a specific structure is formed. One can assume that the thus prepared V–Al–O sample contains largely dispersed, isolated monovanadate species incorporated in an aluminium hydroxide matrix, possibly in tetrahedral coordination. This would explain the deep minimum in the $VO^+/AlOH^+$ ion ratio at pH = 8.5 (Fig. 8e) associated with the lowest coverage of VO_x species on the support, the hydroxylation extent of which is a maximum among the calcined samples (Fig. 8c, d). Low coverage of VO_x species and a high hydroxylation extent of aluminium could also be responsible for the largest C 1s BE shift at pH = 8.5 (Fig. 5c). The enhanced reduction of VO_x species to V^{4+} (Fig. 3b) favors their incorporation in the aluminium hydroxide matrix with a structural transformation that might cause a large drop in the surface area of the dried sample (Fig. 9a) and also gives rise to extreme values of FWHM of the V 2p, Al 2p, O 1s lines (Fig. 4b), of their binding energies (Fig. 5a) and of the VO^+/V^+ ratio (Fig. 8f).

The catalytic behavior of V–Al–O in propane ODH is different from that of alumina-supported vanadia catalysts prepared by incipient wetness impregnation. As was reported by Argyle et al. [35], the initial rate of propene formation per V atom over a VO_x/Al_2O_3 calcined catalyst increased with an increasing vanadia surface density and reached a maximum at $\sim$8 V/nm^2 before decreasing at higher VO_x densities. The increase of the rate with an increasing VO_x surface density was associated with the transformation of low-active dispersed monovanadate species into oligomeric VO_x structures (two-dimensional polyvanadates), whereas the decrease of the rate reflected the introduction of additional vanadia species (crystalline V_2O_5). Tian et al. [38] have shown that with an increase in surface vanadia coverage in a V_2O_5/Al_2O_3 catalyst, isolated surface VO_4 species become polymerized and the fraction of polymeric surface VO_4 species increases until a monolayer coverage is formed ($\sim$8.1 V/nm^2). In the submonolayer region, propane ODH catalytic activity increased with an increasing vanadia surface density and the dependence indicated that only one surface VO_4 site was involved in the rate-determining step for propane ODH to propene. In a similar manner, ethane ODH conversion over the alumina-supported vanadia catalysts increased in this region with an increase in surface vanadia coverage [36]. In vanadium-niobium oxide catalysts prepared by coprecipitation, the rate of propane consumption in the ODH reaction was also observed [39] to increase with an increase in the surface vanadium concentration as determined by low energy ion scattering and XPS; from the dependence it was concluded that the active site on the catalyst surface contained 2.0 $\pm$ 0.3 vanadium atoms on average.

For V–Al–O catalysts, the rates of propane conversion and propene formation decrease with an increase in the surface vanadium concentration, thus implying that polymerized VO_x structures are less active than dispersed isolated monovanadate species. As can be seen from Fig. 13a, the dependence of the activity on the surface V concentration is not general for all the catalysts, but is structure-sensitive. For instance, for the same surface V content, the propene formation rate over calcined catalysts is about twice as large as over dried V–Al–O. Otherwise, the same propene productivity can be achieved for a surface V content about 1.5 times lower in dried catalysts as compared to calcined samples.

On the other hand, the catalytic activity increases with increasing the O/V surface atomic ratio, thus demonstrating the sensitivity to oxygen coordination of V atoms. The dependence of both propane conversion and propene productivity on the O/V ratio is also structure-sensitive and is different for dried and calcined samples (Fig. 13b). However, it turns out that the propane conversion rate for dried V–Al–O and the propene formation rate for calcined catalysts follow practically the same dependence on the O/V ratio. This means that for the same O/V atomic ratio the structural arrangement in dried catalysts is as effective in propane conversion as the structural arrangement in calcined samples for propene formation.

Finally, the rates of propane conversion and propene formation increase with an increase in the surface aluminium concentration. The dependence is nearly general for all catalysts and can be approximated by a power law with an exponent of 4.6–4.7 (Fig. 13c). The obtained

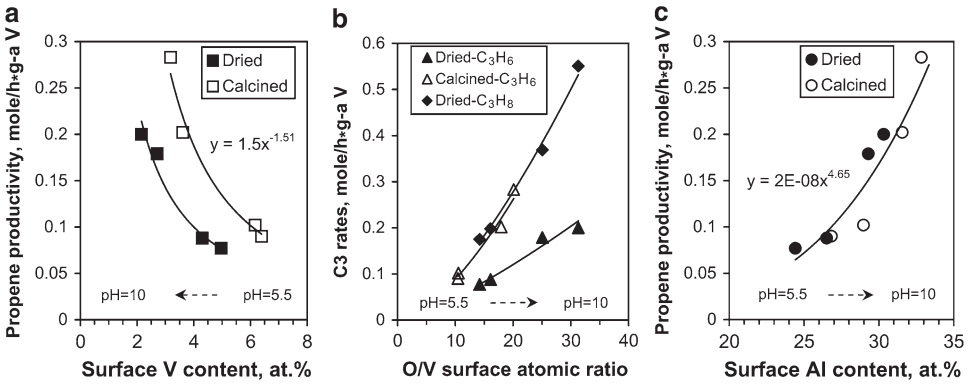

Fig. 13 Variation of the propene formation rate as a function of the XPS-derived V surface concentration (**a**), O/V surface atomic ratio (**b**) and Al surface concentration (**c**) for dried and calcined V–Al–O. In **b**, is also shown the propane conversion rate as a function of the O/V atomic ratio for dried catalysts

dependencies of catalytic activity of V–Al–O on the surface content of the components (Fig. 13) show that the variation of the surface structure and composition caused by different pH and heat treatment is responsible for the variations of the catalytic activity. It seems that V, O and Al atoms altogether are involved in providing active site for propane ODH to propene.

The presence of vanadium lower oxidation states was observed to play an important role in the catalytic process. In particular, the activity of the VO_x/Al_2O_3 catalyst in the dehydrogenation of butanes was related to the presence of the V^{4+} and V^{3+} oxidation states produced by preliminary reduction with H_2, CH_4 and CO [40]. The rate of oxidation of toluene and selectivity for benzaldehyde formation with mixed V_2O_5–WO_3 catalysts was found [41] to correlate with the increase in the amount of V^{4+} species (or $V^{4+}/(V^{5+}+V^{4+}+V^{3+})$ ratio) produced upon reaction, indicating the importance of the V^{4+}/V^{5+} redox couple for high activity and selectivity. The better catalytic properties of $VOPO_4/Al_2O_3$ catalysts as compared to $Fe_{0.23}(VO)_{0.77}PO_4/Al_2O_3$ catalysts in ODH of ethane were attributed [15] to the predominance of surface V^{4+} ions, which could be involved in the ODH reaction through a redox cycle V^{4+}–V^{3+}–V^{4+}. The presence of a great amount of V^{4+} species on the surface of $VOPO_4/TiO_2$ catalysts was presumed to strongly improve their catalytic performances in the ODH of ethane leading to high ethene yields [42]. It has been suggested [32] that the V^{4+} ions present in the V_2O_5/TiO_2–Al_2O_3 catalysts participate in the creation of new strong Lewis-acid sites and strengthening of preexisting sites formed by strong interaction of the low-valence V ions with an alumina component of the mixed support that can affect catalytic properties. On the contrary, Wachs [43] claims that the catalytically active site is the fully oxidized surface VO_4 sites (V^{5+} ions) and not the reduced surface vanadia sites.

According to our data for V–Al–O, the V^{4+} species originally present at the surface of the catalysts can have an influence on their reducibility in hydrogen and the resulting catalytic properties. Indeed, the maximum reduction temperature demonstrates an inverse correlation with the amount of V^{4+} states (cf. Figs. 3b, 9b), which is similar to that shown in Fig. 12b. Though in both dried and calcined catalysts the reduction temperature decreases with an increasing abundance of the V^{4+} oxidation states, the dependence is structure-sensitive: for the same amount of V^{4+} species dried samples (tetrahedral VO_x units) exhibit a better reducibility than calcined V–Al–O (octahedral VO_x units). Better reducibility in a series of dried or calcined V–Al–O corresponds to higher catalytic activity; however, the calcined samples demonstrate better catalytic properties despite worse reducibility and lower surface area as compared to the dried counterpart V–Al–O. When the rate of propane conversion or propene formation is plotted as a function of abundance of the reduced V^{4+} species, a general direct correlation is obtained for all catalysts (Fig. 14a). This means that the presence of reduced V^{4+} species is an important common factor that affects the catalytic properties of all the samples irrespective of their structural state.

It appears that the state of surface oxygen is another general important factor that controls the catalytic activity. In many oxidation reactions, in particular in ODH, the surface oxygen ion has been proposed [44] as a site capable

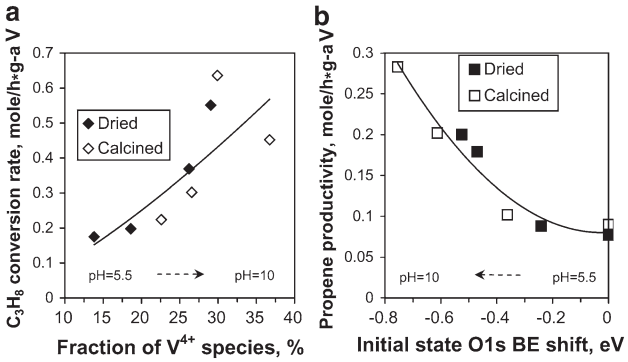

Fig. 14 Correlations between the fraction of reduced V^{4+} species and propane conversion rate (**a**) and between the O 1s binding energy shift caused by the initial state effects ($\Delta E_b^O(\mathrm{ISE}) = k\Delta q^O + \Delta V_M^O$) and propene productivity (**b**) for dried and calcined V–Al–O

of abstracting a hydrogen atom in the form of a proton with the formation of the surface OH group. In this case the activity should depend on the nucleophilicity of surface oxygen, and the extent of charge localization on oxygen may be used as a measure of the surface reactivity with respect to the C–H bond activation. Recently, it has been demonstrated [36, 38] that in alumina-supported vanadia catalysts the oxygen in the bridging V–O–Al bond is the catalytic active site involved in ethane and propane activation during ODH. It was shown [43] that the increase in basicity or electron density of the catalytically active oxygen in the bridging V–O-support bond caused by variation of electronegativity of the support cation enhances its catalytic activity for redox reactions.

Oxygen atoms in V–Al–O are less negative than those in Al_2O_3 and more negative than those in V_2O_5 [17], i.e. they are more nucleophilic in the VO_x units of the catalyst than in vanadia. As the precipitation pH increases, the negative partial charge on oxygen in both dried and calcined V–Al–O rises, as is indicated by a progressive shift of the O 1s peak to lower binding energies which were corrected for the initial state effects (Fig. 5b). Moreover, oxygen in calcined samples turned out to be somewhat more negatively charged than in dried catalysts. Thus, with an increasing pH and after calcination the oxygen sites in V–Al–O become more nucleophilic (basic) and, hence, more active in the propane ODH. This is illustrated by Fig. 14b showing that for all catalysts there is a good correlation between the O 1s BE shift, $\Delta E_b^O(\mathrm{ISE}) = k\Delta q^O + \Delta V_M^O$, caused by the initial state effects and the propene production rate.

5 Conclusions

XPS–SIMS data show that precipitation pH and calcination of V–Al–O catalysts significantly affect their surface physico-chemical state. The surface of dried catalysts obtained in the range of precipitation pH = 5.5–10 is composed of aluminium hydroxide and of dispersed vanadium oxide species mainly in the oxidation state V^{5+} with a fraction of reduced V^{4+} states. The surface of the catalysts is depleted of vanadium in comparison with the bulk. As the precipitation pH increases, the surface atomic concentration of V and O decreases and that of Al increases so that at pH = 10 the V/Al ratio (fixed in the solution at 0.25) drops to 0.078. At the same time the abundance of the V^{4+} species on the surface grows (14–29 %) so that the average oxidation state of vanadium decreases from about +4.86 to +4.71. With an increasing pH the amount of Al hydroxide and the extent of hydroxylation of both V and Al rise; concurrently, the dispersion of vanadium oxide species increases and their coverage of the support decreases.

In the catalysts calcined in air at 500 °C the above compositional trends as a function of pH are largely preserved. At the same time calcination brings about an increase in the surface concentration of V and Al (so that the V/Al atomic ratios approach the bulk values), a decrease in the oxygen surface content and an increase in the relative fraction of reduced V^{4+} species whatever the pH. After calcination the extent of hydroxylation of Al and V decreases and $Al(OH)_3$ transforms largely into AlOOH. Compositional changes induced by variation of pH and heat treatment also give rise to modification of the valence band electronic structure. The calcination causes structural transformations in the vanadium oxide species and aluminum hydroxide/oxyhydroxide support and favors interactions between them, leading to an increasing abundance of the Al–O–V bonds at higher pH. As the pH increases, specific surface area and reducibility increase, exhibiting a correlation with decreasing vanadium surface concentration for both dried and calcined catalysts.

With an increasing pH the catalytic activity of V–Al–O in the propane oxidative dehydrogenation reaction increases; after calcination, catalytic activity increases whatever the pH. The propane conversion rate and propene productivity demonstrate structure-sensitive correlations with the surface concentration of components in dried or calcined catalysts. The activity rises progressively with an increasing population of the V^{4+} species and with an increasing negative partial charge on oxygen atoms, with the dependences being general for all the V–Al–O catalysts. Thus the presence of reduced V^{4+} species and the state of surface oxygen (its nucleophilicity) appear to be important factors that determine the catalytic properties of all the samples irrespective of their structural state.

Acknowledgments This work was carried out under financial support of the Direction Générale des Technologies, de la Recherche et de l'Énergie de la Région Wallonne (GREDECAT). A partial financial support from the National Academy of Sciences of Ukraine in the framework of the Fundamental Research Program "Fundamental Problems of Nanostructural Systems, Nanomaterials, Nanotechnologies-2010" is also acknowledged (S. Ch.).

References

1. Wachs IE, Weckhuysen BM (1997) Appl Catal A 157:67
2. Weckhuysen BM, Keller DE (2003) Catal Today 78:25
3. Mamedov EA, Cortés Corberán V (1995) Appl Catal A 127:1
4. Smits RHH, Seshan K, Leemreize H, Ross JRH (1993) Catal Today 16:513
5. Watling TC, Deo G, Seshan K, Wachs IE, Lercher JA (1996) Catal Today 28:139
6. Wachs IE (2011) Appl Catal A 391:36
7. Pieck CL, Bañares MA, Fierro JLG (2004) J Catal 224:1
8. Shee D, Deo G (2008) Catal Lett 124:340
9. Reddy BM, Chowdhury B, Ganesh I, Reddy EP, Rojas TC, Fernández A (1998) J Phys Chem B 102:10176

10. Reddy BM, Chowdhury B, Reddy EP, Fernández A (2001) Langmuir 17:1132
11. Reddy BM, Ganesh I, Reddy EP, Fernández A, Smirniotis PG (2001) J Phys Chem B 105:6227
12. Reddy BM, Sreekanth PM, Reddy EP, Yamada Y, Xu Q, Sakurai H, Kobayashi T (2002) J Phys Chem B 106:5695
13. Casaletto MP, Lisi L, Mattogno G, Patrono P, Ruoppolo G (2004) Surf Interface Anal 36:737
14. Casaletto MP, Kaciulis S, Lisi L, Mattogno G, Mezzi A, Patrono P, Ruoppolo G (2001) Appl Catal A 218:129
15. Casaletto MP, Lisi L, Mattogno G, Patrono P, Ruoppolo G, Russo G (2002) Appl Catal A 226:41
16. Blangenois N, Florea M, Grange P, Prada Silvy R, Chenakin SP, Bastin JM, Kruse N, Barbero BP, Cadús L (2004) Appl Catal A 263:163
17. Chenakin SP, Prada Silvy R, Kruse N (2011) Metallofiz Noveishie Tekhnol 33:1487
18. Olea M, Florea M, Sack I, Prada Silvy R, Gaigneaux EM, Marin GB, Grange P (2005) J Catal 232:152
19. Florea M, Prada Silvy R, Grange P (2003) Catal Lett 87:63
20. Silversmit G, Poelman H, De Gryse R, Bras W, Nikitenko S, Florea M, Grange P, Delsarte S (2006) Catal Today 118:344
21. Safonova OV, Florea M, Bilde J, Delichere P, Millet JMM (2009) J Catal 268:156
22. Florea M, Prada Silvy R, Grange P (2005) Appl Catal A 286:1
23. Chenakin SP, Prada Silvy R, Kruse N (2005) J Phys Chem B 109:14611
24. Chenakin SP, Prada Silvy R, Kruse N (2007) Surf Interface Anal 39:567
25. Rotole JA, Sherwood PMA (1999) J Vac Sci Technol A 17:1091
26. Kloprogge JT, Duong LV, Wood BJ, Frost RL (2006) J Colloid Interface Sci 296:572
27. Böse O, Kemnitz E, Lippitz A, Unger WES (1997) Fresenius J Anal Chem 358:175
28. Alexander MR, Thompson GE, Beamson G (2000) Surf Interface Anal 29:468
29. Mendialdua J, Casanova R, Barbaux Y (1995) J Electron Spectrosc Relat Phenom 71:249
30. Silversmit G, Depla D, Poelman H, Marin GB, De Gryse R (2004) J Electron Spectrosc Relat Phenom 135:167
31. Moretti G (1998) J Electron Spectrosc Relat Phenom 95:95
32. Matralis HK, Ciardelli M, Ruwet M, Grange P (1995) J Catal 157:368
33. Sawatzky GA, Post D (1979) Phys Rev B 20:1546
34. Demeter M, Neumann M, Reichelt W (2000) Surf Sci 41:454
35. Argyle MD, Chen K, Bell AT, Iglesia E (2002) J Catal 208:139
36. Martínez-Huerta MV, Gao X, Tian H, Wachs IE, Fierro JLG, Bañares MA (2006) Catal Today 118:279
37. Santacesaria E, Cozzolino M, Di Serio M, Venezia AM, Tesser R (2004) Appl Catal A 270:177
38. Tian H, Ross EI, Wachs IE (2006) J Phys Chem B 110:9593
39. Smits RHH, Seshan K, Ross JRH, van den Oetelaar LCA, Helwegen JHJM, Anantharaman MR, Brongersma HH (1995) J Catal 157:584
40. Harlin ME, Niemi VM, Krause AOI (2000) J Catal 195:67
41. Yan Z-G, Andersson SLT (1990) Appl Catal 66:149
42. Casaletto MP, Lisi L, Mattogno G, Patrono P, Ruoppolo G (2004) Appl Catal A 267:157
43. Wachs IE (2005) Catal Today 100:79
44. Zhdan PA, Shepelin AP, Osipova ZG, Sokolovskii VD (1979) J Catal 58:8